A Combined-Slip Physical Tire Model Based on the Vector Distribution Considering Tire Anisotropic Stiffness

**Ye Zhuang · Zhanshuai Song · Xueliang Gao ·
Xiaoguang Yang · Weiping Liu**

Abstract The tire mechanics characteristics exert significant influence on vehicle dynamics and control, especially under the combined cornering/braking/driving conditions. In general, tire steady-state mechanics models can be divided into three categories: empirical models, semi-empirical models, and physical models. Compared with empirical model and semi-empirical model, the physical model is more suitable for theoretical derivation and analytical solution in vehicle dynamics research, especially under the extreme conditions of large slip, such as drift cornering. Therefore, a physical predictive tire model with high accuracy and simplified expression has been proposed in the paper, which avoids the complex tire testing for the combined-slip conditions. The Exact Unified Combine Brush (EUCB for short) model proposed is based on the brush model and the vector distribution principle considering anisotropic tire stiffness. The brush model,

as a theoretical basis of many tire models, could analytically and qualitatively explain many tire mechanics phenomena. The vector distribution could accurately describe the magnitude and direction of the shear forces from the physical sense under the combined lateral and longitudinal slip conditions. In the paper, the derivation process of the proposed model is introduced firstly from pure and combined slip conditions. Then, comparison between the brush physical models based on three assumptions about the direction of resultant shear force and the proposed model is separately conducted. Lastly, the proposed model is compared with the COMBINATOR model, Magic Formula (MF for short) model and Modified Dugoff model, and validated by the test data under different conditions. The result shows that the proposed model has good accuracy and predictive ability.

Y. Zhuang · Z. Song
State Key Laboratory of Automotive Simulation and
Control, Changchun, Jilin 130025, China

X. Gao
School of Mechatronic Engineering, Changchun University
of Technology, Changchun, Jilin 130012, China

X. Yang
Vanlead Rubber & Tire Research Institute, Wanli Tire
Corporation Limited, Guangzhou, Guangdong 510425,
China

W. Liu (✉)
College of Instrumentation & Electrical Engineering, Jilin
University, Changchun, Jilin 130061, China
e-mail: liuweiping2014@jlu.edu.cn

1 Introduction

As the primary interactive force media between the road vehicle and the ground, the tires play the fundamental role in vehicle dynamics and control research [1–4]. Vehicle braking safety, handling stability, vertical vibration and front wheel shimmy characteristics all depend on the study of tire mechanics characteristics. The design and development of the chassis control

system (such as Antilock Brake System, Traction Control System, Direct Yaw Control, etc.) are based on the study of tire mechanical characteristics [5–7].

The study of tire mechanical properties first starts from the pure cornering condition, and then extends to the combined cornering/braking/driving conditions [4]. Compared with the pure-slip tire model, the combined-slip tire model could accurately describe the coupling relationship between longitudinal and lateral forces. Therefore, the tire model under the combined conditions have been studied extensively since the 1930's [7]. In general, tire steady-state mechanics models can be divided into three categories: empirical models, semi-empirical models, and physical models [7]. In addition, there are some methods to obtain tire forces, such as finite-element method and Gaussian process regression [8–10]. The empirical model is directly obtained from tire test data, so the accuracy of the model is high. However, due to the lack of theoretical foundation, the model's extrapolation and theoretical accuracy are poor [7]. As the most popular empirical tire model, the MF model could express the tire forces and moments accurately in combined-slip conditions [5,6,11], while it needs a mass of test data to identify the parameters of the model which is time-consuming and complicated in practice.

The semi-empirical model is modeled on the basis of theoretical research and experimental analysis. Thus, the semi-empirical model not only has high theoretical accuracy, good extrapolation, but also has high simulation accuracy [7]. At present, the typical semi-empirical model is the UniTire model [12–16]. Compared with the MF model, the UniTire model has better predictive ability, better theoretical accuracy, and fewer parameters.

The physical model is a mathematical description of the tire's mechanical characteristics based on tire's physical structure and deformation mechanism [7]. The model is of great significance for analyzing the physical nature of tire mechanics and studying the influence of structural parameters on the mechanical properties. Compared with empirical model and semi-empirical model, the physical model is more suitable for theoretical derivation and analytical solution in vehicle dynamics research, especially under the extreme conditions of large slip, such as drifting [7,17]. However, there are two main problems in the current physical models. One is that the model is too complicated to be applied in actual vehicle dynamics research [18,19]. The other is

that the accuracy of the model is not high due to many simplifications in the modeling process such as Dugoff model [20–23]. As we all know, it is difficult to obtain the data of combined slip conditions, which requires expensive cost and a long test period. The predictive model can use the tire test data under pure slip conditions to predict the tire forces under combined slip conditions. Thus, it is necessary to develop a physical predictive model with high accuracy and simplified expression.

When modeling the tire combined-slip maneuvers, the allocation of the resultant shear force between the lateral and longitudinal direction has to be determined. The accuracy of the allocation would greatly affect the combined model results. In most of the combined-slip tire models available, the direction of the resultant force, or the tangent angle between the lateral and the longitudinal force, is determined by the ratio of lateral slip rate vs longitudinal slip rate [24,25], such as COMBINATOR model [25]. To account the difference of the allocation in the adhesion region and sliding region within the contact patch, the UniTire model utilizes different allocation expression in the two regions and introduces a factor to express the transition from adhesion to sliding state. In this way, the model could express the combined-slip forces with better accuracy [12–16], while the exact allocation under arbitrary condition still need to be established to theoretically and exactly express the combined-slip tire mechanics. Therefore, a novel distribution principle for the combined-slip tire modelling is proposed by accounting the anisotropic tire stiffness and friction coefficient to calculate the shear forces accurately under lateral and longitudinal slip conditions.

In the paper, a physical predictive model is proposed based on the unified combine brush model which can describe the tire forces accurately under lateral and longitudinal slip conditions. Firstly, the derivation process of proposed model is introduced from pure and combined slip conditions. Then, comparison between the brush physical models based on three assumptions about the direction of resultant shear force and the proposed model is separately conducted to explain the correctness of the model in theory. Lastly, the proposed tire model is compared with COMBINATOR model, MF model and Modified Dugoff model and verified by test data under different conditions.
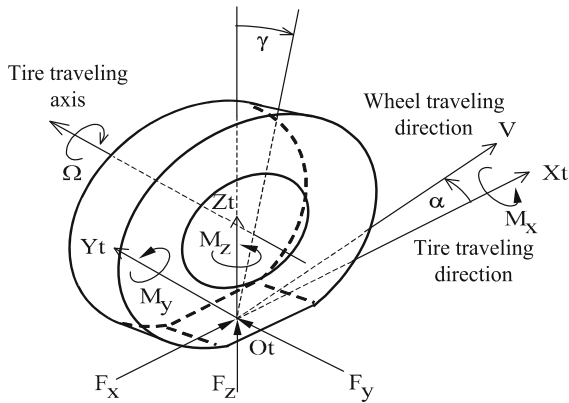
Fig. 1 Tire coordinate system in [10]

Fig. 2 Deformation of the bristles in contact patch under pure lateral slip condition

2 The foundation of modeling

2.1 Tire coordinate system

The Tire Contact Process coordinate is employed to describe the longitudinal and lateral slip ratio uniformly [13], as shown in Fig. 1. The Centre of contact patch is defined as the origin of coordinate system. The coordinate axes with positive direction are shown above, and more details are described in Ref. [13]. The velocity of wheel is shown as V, and γ is the inclination angle, and the slip angle α is angle between Xt-axis and the direction of the velocity of wheel. The figure above shows the six-component force within the contact patch, whose direction denotes positive. The main topic in the paper is calculation of shear forces under combined slip conditions, so three moments are not discussed.

2.2 The slip ratios

The slip ratios are defined as the sliding speed over the rolling speed as shown below [13].

$$\begin{cases} S_x = \dfrac{-V_{sx}}{V_r} = -\dfrac{V\cos\alpha - \Omega R_e}{\Omega R_e} & S_x \in (-\infty, +\infty) \\ S_y = \dfrac{-V_{sy}}{V_r} = -\dfrac{V\sin\alpha}{\Omega R_e} & S_y \in (-\infty, +\infty) \end{cases}$$
(1)

where S_x is the longitudinal slip ratio, S_y is the lateral slip ratio, V_{sx} is the longitudinal slip velocity of tire to the road surface, V_{sy} is the lateral slip velocity to the road surface, V_r is the rolling velocity, V is the wheel
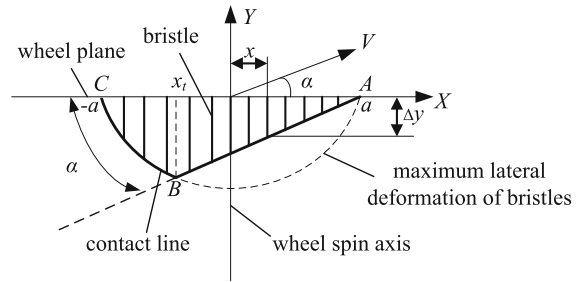
velocity, α is the slip angle, R_e is the effective rolling radius of tire, and Ω is the rolling angular speed.

In practical test, the longitudinal slip ratio κ [13] is often used instead of Sx and its expression is:

$$\kappa = \frac{-V_{sx}}{V\cos\alpha} = -\frac{V\cos\alpha - \Omega R_e}{V\cos\alpha}$$
(2)

2.3 The pressure distribution within tire contact patch

A parabolic distribution on vertical load over the contact patch is adopted in the work for simplifying the process of tire analytical modeling. And this distribution pattern can approximately express the pressure distribution under small load and is not suitable for pressure distribution under overload and heavy load. The distribution of the load per unit length is expressed as follows:

$$q_z = \frac{3F_z}{4a}\left[1 - \left(\frac{x}{a}\right)^2\right] \quad x \in (-a, a)$$
(3)

where F_z is the vertical force and a is the half of the contact length $2a$ [6].

3 The physical model for pure slip

The proposed model gets started from pure slip conditions. The model under pure slip condition is similar to the model in Ref. [6], and the two models are different in expressions. The derivation process of pure lateral slip condition is shown as follows.

Figure 2 shows the deformation of bristles in contact patch under pure lateral slip condition, where 'ABC' is the contact line of bristles with the ground. The whole contact patch is divided into adhesion region 'AB' and sliding region 'BC', and 'B' is the initial sliding point.

According to Fig. 2, the lateral deformation [7] of the tread elements in the adhesion region is:

$$\Delta y = (a - x) \cdot S_y = -(a - x) \cdot \tan \alpha \qquad (4)$$

And the lateral shear stress [7] in contact patch of elastic bristles is

$$q_y = k_{ty} \cdot S_y \cdot (a - x) \quad x \in (-a, a) \qquad (5)$$

where k_{ty} is lateral stiffness of the bristles per unit length.

When the magnitude of shear stress above is equal to the maximum friction force, the coordinate of initial sliding points x_t meets the equation below [5]:

$$|k_{ty} \cdot S_y \cdot (a - x_t)| = \mu_y \cdot q_z \qquad (6)$$

where μ_y is the lateral friction coefficient. Solving the equation above, it yields the coordinate of initial sliding points:

$$x_t = 2a \frac{k_y |S_y|}{3 \mu_y F_z} - a \quad x_t \in (-a, a) \qquad (7)$$

When x_t equals to a, the whole sliding condition is:

$$\alpha_{sl} = \arctan\left(\frac{3 \mu_y F_z}{k_y}\right) \qquad (8)$$

where k_y is the cornering stiffness of tire and α_{sl} is the slip angle where whole sliding stars.

The normalized lateral slip ratio ϕ_y [7] is introduced to express the lateral force briefly:

$$\phi_y = \frac{k_y S_y}{\mu_y F_z} \quad \phi_y \in (-\infty, +\infty) \qquad (9)$$

If the slip angle is given, the lateral force of tire can be yield by the expression below.

$$F_y = \begin{cases} \int_{x_t}^{a} k_{ty} S_y (a - x) dx + \int_{-a}^{x_t} \mu_y q_z dx & |\alpha| \leq \alpha_{sl} \\ \int_{-a}^{a} \mu_y q_z dx & |\alpha| > \alpha_{sl} \end{cases}$$
$$= \begin{cases} \mu_y F_z \cdot \phi_y \cdot (1 - \frac{1}{3}|\phi_y| + \frac{1}{27}\phi_y^2) & |\alpha| \leq \alpha_{sl} \\ \mu_y F_z \cdot \phi_y \cdot (1 - \frac{1}{3}|\phi_y| + \frac{1}{27}\phi_y^2) & |\alpha| > \alpha_{sl} \end{cases}$$
$$\qquad (10)$$

The derivation process of the model under pure longitudinal slip condition is similar to the process above, so it's not stated here. The longitudinal shear force under pure longitudinal slip condition is shown as follows:
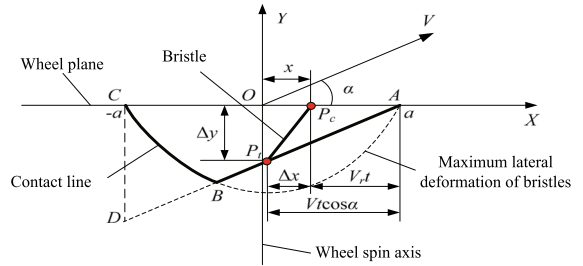

Fig. 3 Deformation of the bristles in contact patch under the combined conditions in [7]

$$F_x = \begin{cases} \mu_x F_z \cdot \phi_x \cdot (1 - \frac{1}{3}|\phi_x| + \frac{1}{27}\phi_x^2) & |S_x| \leq S_{xsl} \\ \mu_x F_z \cdot sign(S_x) & |S_x| > S_{xsl} \end{cases}$$
$$\qquad (11)$$

where ϕ_x is the normalized longitudinal slip ratio [7], and its expression is:

$$\phi_x = \frac{k_x S_x}{\mu_x F_z} \quad \phi_x \in (-\infty, +\infty) \qquad (12)$$

And S_{xsl} is the longitudinal slip ratio where whole sliding stars, and its expression is shown below:

$$S_{xsl} = 3 \mu_x F_z / k_x \qquad (13)$$

where k_x is the longitudinal slip stiffness of tire and μ_x is longitudinal friction coefficient.

4 The physical model for combined slip

4.1 The derivation of the exact unified combined brush model

How to distribute accurately the longitudinal force and lateral force is a main problem in combined model. Whether the resultant force direction is assumed to be the same as that in sliding region, or adhesion region, they are not suitable when the tire is anisotropic [13]. Therefore, based on the vector distribution principle considering anisotropic tire stiffness, the exact unified combined brush model (EUCB model for short) could describe accurately the variation of the shear forces. The derivation process of combined slip condition is shown as follows.

Figure 3 shows the deformation of bristles in contact patch under combined cornering and braking condition [7]. The shear stresses [7] of point P_t in X and Y directions under combined conditions is:

$$\mathbf{q} = \begin{bmatrix} q_x \\ q_y \end{bmatrix} = \begin{bmatrix} k_{tx} \cdot \Delta x \\ k_{ty} \cdot \Delta y \end{bmatrix}$$
$$= \begin{bmatrix} k_{tx} \cdot S_x \cdot (a - x) \\ k_{ty} \cdot S_y \cdot (a - x) \end{bmatrix} \quad x \in (-\infty, +\infty) \quad (14)$$

The magnitude of total shear stress [7] is:

$$q = (a - x) \cdot \sqrt{(k_{tx} S_x)^2 + (k_{ty} S_y)^2} \quad (15)$$

Solving the balance equation $q(x_t) = \mu^a \cdot q_z(x_t)$, the coordinate of initial sliding points could be yield:

$$x_t = 2a \cdot \phi/3 - a \quad x_t \in (-a, a) \quad (16)$$

where ϕ is the normalized combined slip ratio with expression $\phi = \sqrt{\phi_x^2 + \phi_y^2}$ and μ^a is the directional friction coefficient of adhesion region, and its expression is shown below which can be obtained through the friction ellipse concept [13].

$$\mu^a = \sqrt{\left(\mu_x \frac{\phi_x}{\phi}\right)^2 + \left(\mu_y \frac{\phi_y}{\phi}\right)^2} \quad (17)$$

Integrating the magnitude of shear stress in adhesion region, the magnitude of shear force in adhesion region can be obtained:

$$F^a = \sqrt{(k_x S_x)^2 + (k_y S_y)^2} \cdot (1 - \phi/3)^2 \quad (18)$$

Integrating the magnitude of shear stress in sliding region, the magnitude of shear force in the region is:

$$F^s = \mu^s F_z \cdot \phi^2 \cdot (1/3 - 2\phi/27) \quad (19)$$

where μ^s is the directional friction coefficient of sliding region, and its expression can be also obtained through the friction ellipse concept.

Figure 4 shows the vector distribution relationship among normalized shear forces under two assumptions, with one considering the anisotropy of tire stiffness and the other not. When the longitudinal slip stiffness of the tire is different from the cornering stiffness, the direction of shear force in sliding region and that in adhesion region are different as shown in Fig. 4b [14,15]. Therefore, it is inaccurate that the direction of resultant shear force is assumed to be the same as the direction of shear force in sliding region or adhesion region with ignoring the anisotropy of tire stiffness as described in Fig. 4a [14,15].
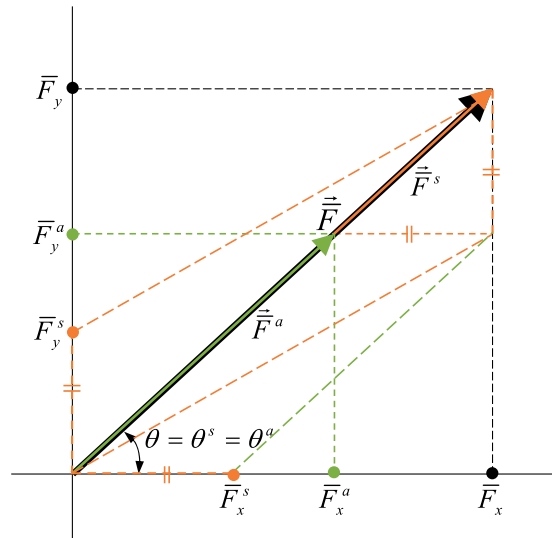
(a) considering isotropic tire stiffness
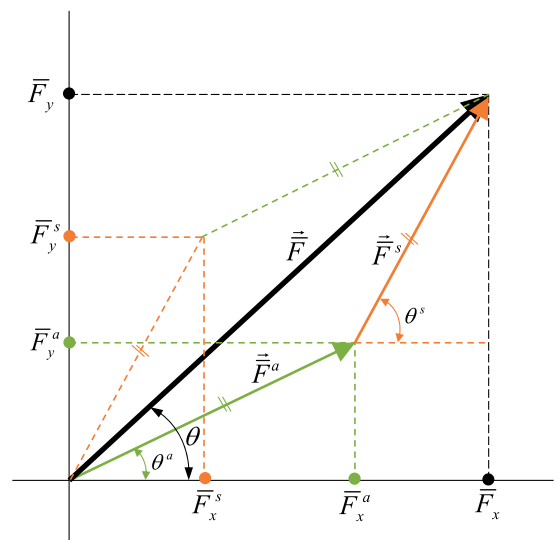
(b) considering anisotropic tire stiffness

Fig. 4 Vector distribution relationship among normalized shear forces

And the meaning of each symbol is explained below. The normalized resultant shear force, longitudinal force and lateral force in adhesion region can be yielded as follows:

$$\bar{F}^a = \frac{F^a}{\mu^a F_z}, \quad \bar{F}_x^a = \frac{F_x^a}{\mu_x F_z}, \quad \bar{F}_y^a = \frac{F_y^a}{\mu_y F_z} \quad (20)$$

where F^a is the absolute magnitude of its own vector $\mathbf{F^a}$ and F_x^a, F_y^a are longitudinal and lateral forces in adhesion region. The vector $\bar{\mathbf{F}}^a$ can be expressed as ($\bar{F}_x^a$, $\bar{F}_y^a$).

In the same way, the normalized forces in sliding region can be obtained:

$$\bar{F}^s = \frac{F^s}{\mu^s F_z}, \quad \bar{F}_x^s = \frac{F_x^s}{\mu_x F_z}, \quad \bar{F}_y^s = \frac{F_y^s}{\mu_y F_z} \tag{21}$$

where F^s is the absolute magnitude of its own vector and F_x^s, F_y^s are longitudinal and lateral forces in the region. The vector $\bar{\mathbf{F}}^s$ can be expressed as ($\bar{F}_x^s$, $\bar{F}_y^s$).

Combining Eqs. (20)–(21) and Fig. 4b, the following equations can be obtained obviously:

$$\bar{F}_x = \bar{F}_x^a + \bar{F}_x^s, \quad \bar{F}_y = \bar{F}_y^a + \bar{F}_y^s, \quad \bar{\mathbf{F}} = \bar{\mathbf{F}}^a + \bar{\mathbf{F}}^s \tag{22}$$

$$\begin{cases} \bar{F}^a = \sqrt{(\bar{F}_x^a)^2 + (\bar{F}_y^a)^2} \\ \bar{F}^s = \sqrt{(\bar{F}_x^s)^2 + (\bar{F}_y^s)^2} \\ \bar{F} = \sqrt{(\bar{F}_x)^2 + (\bar{F}_y)^2} \end{cases} \tag{23}$$

where $\bar{F}_x$, $\bar{F}_y$ and $\bar{F}$ are normalized longitudinal force, lateral force and resultant shear force respectively. And the vector $\bar{\mathbf{F}}$ can be expressed as ($\bar{F}_x$, $\bar{F}_y$).

From the above equations, the longitudinal and lateral forces in contact patch are:

$$F_x = F_x^a + F_x^s = \mu_x F_z(\bar{F}_x^a + \bar{F}_x^s) \tag{24}$$
$$F_y = F_y^a + F_y^s = \mu_y F_z(\bar{F}_y^a + \bar{F}_y^s) \tag{25}$$

And the directions of normalized shear forces in adhesion region and sliding region are, respectively:

$$\tan(\theta^a) = \frac{\bar{F}_y^a}{\bar{F}_x^a} = \frac{\phi_y}{\phi_x}, \quad \tan(\theta^s) = \frac{\bar{F}_y^s}{\bar{F}_x^s} = \frac{\phi_y}{\phi_x} \cdot \frac{k_x}{k_y} \tag{26}$$

And the direction of normalized shear force is:

$$\tan(\theta) = \frac{\bar{F}_y}{\bar{F}_x} = \frac{\bar{F}_y^a + \bar{F}_y^s}{\bar{F}_x^a + \bar{F}_x^s} \tag{27}$$

Therefore, the longitudinal force and lateral force of the tire in contact patch can be obtained as follows and the expressions correspond to two conditions. One is that the contact patch is covered by sliding region entirely with $\phi > 3$, the other is that there is adhesion region in contact patch with $0 \leq \phi \leq 3$.

$$\begin{cases} \begin{cases} F_x = \mu_x F_z(\bar{F}^a \dfrac{\phi_x}{\phi} + \bar{F}^s \dfrac{\phi_x \cdot k_y/k_x}{\sqrt{\phi_y^2 + (\phi_x \cdot k_y/k_x)^2}}) \\ \qquad\qquad\qquad\qquad 0 \leq \phi \leq 3 \\ F_y = \mu_y F_z(\bar{F}^a \dfrac{\phi_y}{\phi} + \bar{F}^s \dfrac{\phi_y}{\sqrt{\phi_y^2 + (\phi_x \cdot k_y/k_x)^2}}) \end{cases} \\ \begin{cases} F_x = \mu_x F_z \dfrac{\phi_x \cdot k_y/k_x}{\sqrt{\phi_y^2 + (\phi_x \cdot k_y/k_x)^2}} \\ \qquad\qquad\qquad\qquad \phi > 3 \\ F_y = \mu_y F_z \dfrac{\phi_y}{\sqrt{\phi_y^2 + (\phi_x \cdot k_y/k_x)^2}} \end{cases} \end{cases} \tag{28}$$

where the normalized shear force in adhesion region is $\bar{F}^a = \phi \cdot (1 - \phi/3)^2$, and the normalized shear force in sliding region is $\bar{F}^s = \phi^2 \cdot (1/3 - 2\phi/27)$.

4.2 The simulation and analysis of the exact unified combined brush model

The longitudinal force and lateral force of tire can be found through the formula (28) with given friction characteristic parameters, tire's speed, longitudinal slip rate, slip angle and basic characteristic parameters under combined conditions.

To validate the EUCB model, the simulation results are compared with the brush physical tire model based on the arbitrary pressure distribution with three different assumptions about the direction of resultant shear force. Currently, the three direction assumptions are: the direction of resultant shear force is consistent with that in adhesion region which is $\frac{F_y}{F_x} = \frac{k_y S_y}{k_x S_x}$, the direction of resultant shear force is consistent with that in sliding region which is $\frac{F_y}{F_x} = \frac{S_y}{S_x}$, and the direction of resultant shear force transitions from that in adhesion region to sliding region as the slip rate increases which is $\frac{F_y}{F_x} = \frac{k_y S_y}{\lambda k_x S_x}$, where λ is the direction factor and its expression is:

$$\lambda = 1 + (k_y/k_x - 1)\bar{F} \tag{29}$$

In simulation, tire speed is 80km/h, tire friction characteristic parameters are: $\mu_x = 1$, $\mu_y = 0.7$, basic characteristic parameters of tire are: $k_x = 90$KN/rad, $k_y = 40$KN/rad, $F_z = 5000$N, $R_e = 0.4$m, $a = 12.55$cm, where R_e is the effective radius of tire. And
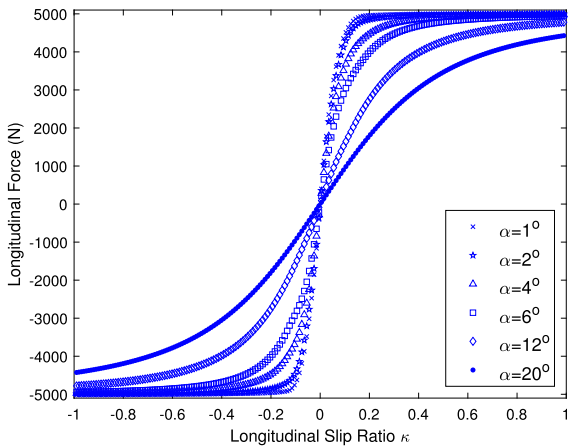
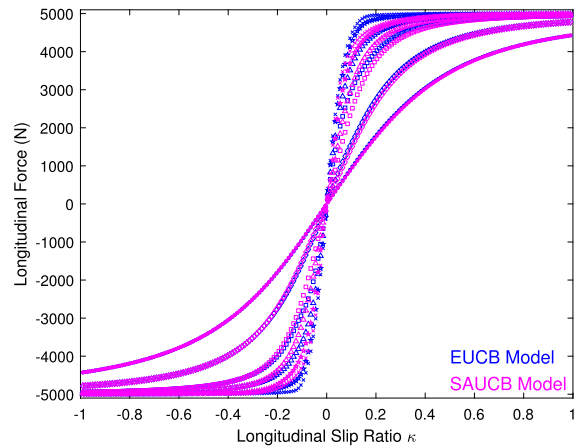**Fig. 5** Longitudinal force vs. kappa under different slip angles

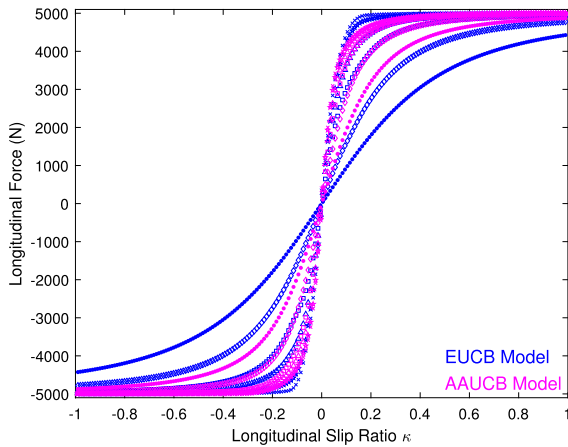**Fig. 7** Longitudinal force comparisons between EUCB model and SAUCB model

Fig. 6 Longitudinal force comparisons between EUCB model and AAUCB model
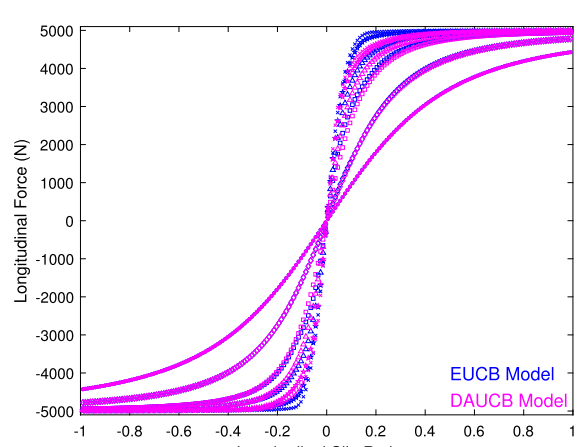

Fig. 8 Longitudinal force comparisons between EUCB model and DAUCB model

the brush models based on the three assumptions above are short for AAUCB, SAUCB, and DAUCB model, respectively.

Figure 5 shows the longitudinal force calculated by the EUCB model at 6 slip angles. Figures 6, 7 and 8 show the comparisons of longitudinal force calculated by the EUCB model and the brush models based on the three assumptions above. It can be seen that the EUCB model and AAUCB model have similar effect on expressing longitudinal force under small longitudinal slip ratio and small slip angle, while the EUCB model and SAUCB model or DAUCB model have nearly consistent effect on describing longitudinal force under large slip conditions. The comparison results indicate the EUCB model has high accuracy on describing longitudinal force under various slip conditions.
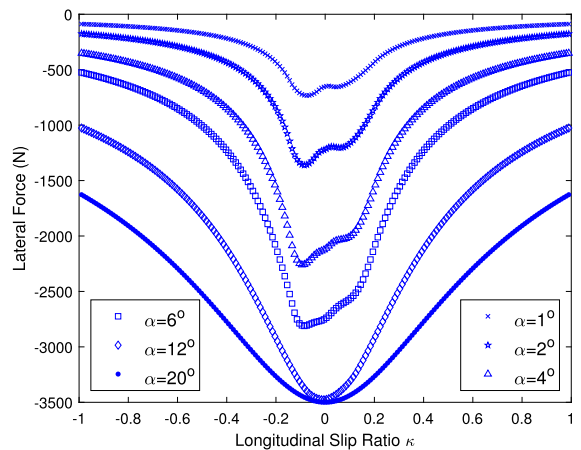

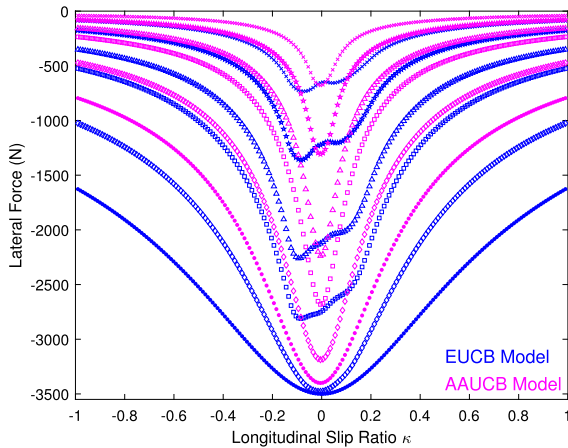**Fig. 9** Lateral force vs. kappa under different slip angles

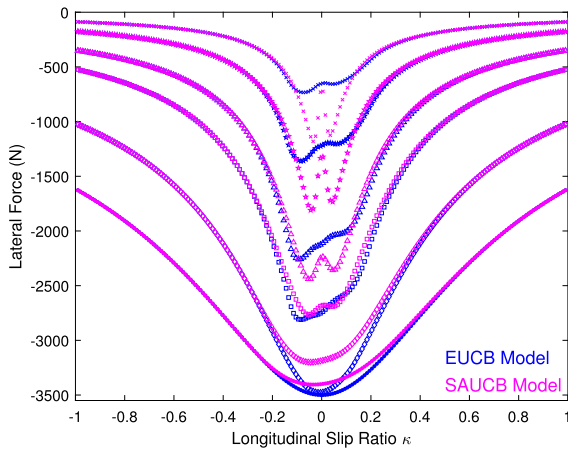**Fig. 10** Lateral force comparisons between EUCB model and AAUCB model

Fig. 11 Lateral force comparisons between EUCB model and SAUCB model
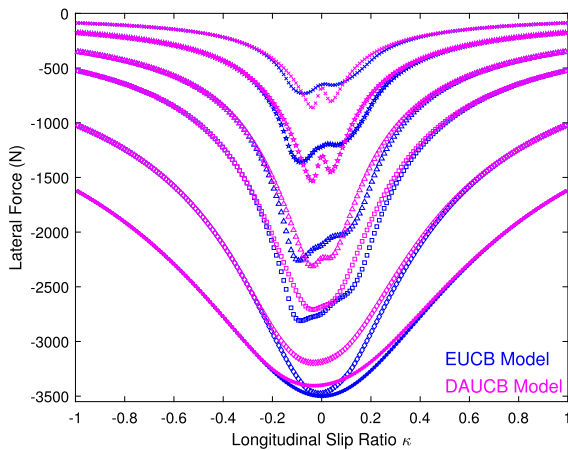

Fig. 12 Lateral force comparisons between EUCB model and DAUCB model

Figure 9 shows the lateral force calculated by the EUCB model at 6 slip angles. From the fig, it can be seen that the model exists 'double peaks' under small slip angles, and the peak value of the braking side is greater than the peak value of the driving side, which conforms to the characteristics of the double peak phenomenon [7].

Figures 10, 11 and 12 show the comparisons of lateral force calculated by the EUCB model and the brush models based on the three assumptions above. From the figures, it can be seen that the EUCB model and AAUCB model have obvious difference on describing lateral force and the difference increases as slip increases. And the EUCB model and SAUCB model or DAUCB model are nearly consistent on describing longitudinal force under large slip conditions. The comparison results show that the EUCB model could describe accurately the direction variation of shear force and express accurately the longitudinal and lateral force with anisotropic tire stiffness and friction coefficient.

4.3 The introduction of dynamic friction coefficient

Many test data indicate that the force and moment of the tire would be affected by the speed-dependent friction feature, which is particularly significant under large slip condition [26–28]. Therefore, the dynamic friction coefficient is introduced into the combined model. The longitudinal and lateral friction coefficients [28] are as follows.

$$
\begin{cases}
\mu_x = \mu_{dx} + (\mu_{sx} - \mu_{dx}) \\
\quad \cdot \exp\left\{ -h_x^2 \cdot \lg^2\left[\left| \dfrac{V_{sx}}{V_{mx}} \right| + \exp\left(-\dfrac{V_{sx}}{V_{mx}} \right) \right] \right\} \\
\mu_y = \mu_{dy} + (\mu_{sy} - \mu_{dy}) \\
\quad \cdot \exp\left\{ -h_y^2 \cdot \lg^2\left[\left| \dfrac{V_{sy}}{V_{my}} \right| + \exp\left(-\dfrac{V_{sy}}{V_{my}} \right) \right] \right\}
\end{cases}
\tag{30}
$$

where μ_{dx}, μ_{sx}, h_x and V_{mx} are longitudinal parameters and μ_{dy}, μ_{sy}, h_y and V_{my} are lateral parameters of the friction model. When V_{sx} and V_{sy} are zeros, μ_{sx} equals μ_x and μ_{sy} equals μ_y, so μ_{sx} and μ_{sy} are static friction coefficients [26]. When V_{sx} and V_{sy} tend to infinity, μ_{dx} equals μ_x and μ_{dy} equals μ_y.

Figure 13 shows the schematic diagram of the stress distribution in contact patch with dynamic friction coef-
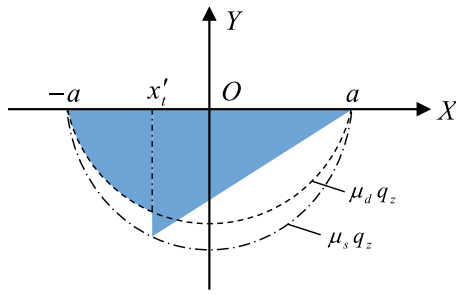
Fig. 13 Schematic diagram of the stress distribution in contact patch with dynamic friction

ficient, and μ_s represents the static friction coefficient and μ_d represents the dynamic friction coefficient.

The introduction of dynamic friction coefficient mainly causes the changes of the starting slip condition and initial sliding point. For the pure lateral slip condition, the starting slip condition becomes:

$$|q_y| = \mu_{sy} \cdot q_z \tag{31}$$

and the initial sliding point becomes:

$$x'_t = 2a\frac{k_y|S_y|}{3\mu_{sy}F_z} - a \qquad x'_t \in (-a, a) \tag{32}$$

When $x'_t = a$, the total sliding condition becomes:

$$|\alpha| = \alpha'_{sl} = \arctan(3\mu_{sy}F_z/k_y) \tag{33}$$

Then the expression of the lateral shear force is as follows:

$$F_y = \begin{cases} \dfrac{\phi'_y}{3} \cdot F_z \cdot [3\mu_{sy}(1 - \dfrac{|\phi'_y|}{3})^2 \\ + \mu_y \cdot (|\phi'_y| - \dfrac{2}{9}\phi'^2_y)] & |\alpha| \le \alpha'_{sl} \\ -\mu_y F_z \cdot sign(\alpha) & |\alpha| > \alpha'_{sl} \end{cases} \tag{34}$$

where ϕ'_y is expressed as:

$$\phi'_y = \frac{\mu_y}{\mu_{sy}}\phi_y = \frac{k_y S_y}{\mu_{sy}F_z} \tag{35}$$

Similarly, the longitudinal shear force under pure longitudinal slip condition becomes:

$$F_x = \begin{cases} \dfrac{\phi'_x}{3} \cdot F_z \cdot [3\mu_{sx}(1 - \dfrac{|\phi'_x|}{3})^2 \\ + \mu_x \cdot (|\phi'_x| - \dfrac{2}{9}\phi'^2_x)] & |S_x| \le S'_{xsl} \\ \mu_x F_z \cdot sign(S_x) & |S_x| > S'_{xsl} \end{cases} \tag{36}$$

where ϕ'_x is expressed as:

$$\phi'_x = \frac{\mu_x}{\mu_{sx}}\phi_x = \frac{k_x S_x}{\mu_{sx}F_z} \tag{37}$$

and the longitudinal slip ratio where whole sliding stars becomes S'_{xsl}, and its expression is below:

$$S'_{xsl} = 3\mu_{sx}F_z/k_x \tag{38}$$

For the combined slip condition with considering dynamic friction coefficient, the starting slip condition becomes:

$$q(x'_t) = \mu_s \cdot q_z(x'_t) \tag{39}$$

Solving the equation above, the coordinate of initial sliding point is as follows:

$$x'_t = 2a \cdot \phi'/3 - a \qquad x_t \in (-a, a) \tag{40}$$

When ϕ' is greater than 3, there is no adhesion region in the contact path and its expression is

$$\phi' = \phi \cdot \mu^a/\mu_s \tag{41}$$

where μ_s is static friction coefficient, similarly, its expression can be obtained through the friction ellipse concept.

$$\mu_s = \sqrt{\left(\mu_{sx}\frac{\phi_x}{\phi}\right)^2 + \left(\mu_{sy}\frac{\phi_y}{\phi}\right)^2} \tag{42}$$

From the content above, the longitudinal force and lateral force of the tire with considering the dynamic friction coefficient under combined condition become:

$$\begin{cases} \begin{cases} F_x = \mu_x F_z(\bar{F}^{a'}\dfrac{\phi_x}{\phi} + \bar{F}^{s'}\dfrac{\phi_x \cdot k_y/k_x}{\sqrt{\phi_y^2 + (\phi_x \cdot k_y/k_x)^2}}) \\ \qquad\qquad\qquad\qquad 0 \le \phi' \le 3 \\ F_y = \mu_y F_z(\bar{F}^{a'}\dfrac{\phi_y}{\phi} + \bar{F}^{s'}\dfrac{\phi_y}{\sqrt{\phi_y^2 + (\phi_x \cdot k_y/k_x)^2}}) \end{cases} \\ \begin{cases} F_x = \mu_x F_z\dfrac{\phi_x \cdot k_y/k_x}{\sqrt{\phi_y^2 + (\phi_x \cdot k_y/k_x)^2}} \\ \qquad\qquad\qquad\qquad \phi' > 3 \\ F_y = \mu_y F_z\dfrac{\phi_y}{\sqrt{\phi_y^2 + (\phi_x \cdot k_y/k_x)^2}} \end{cases} \end{cases} \tag{43}$$

where the normalized shear force in adhesion region is $\bar{F}^{s'} = \phi'^2 \cdot (1/3 - 2\phi'/27))$, and the normalized shear force in sliding region is $\bar{F}^{a'} = \phi \cdot (1 - \phi'/3)^2$.

5 Experiment validation

5.1 Test data used

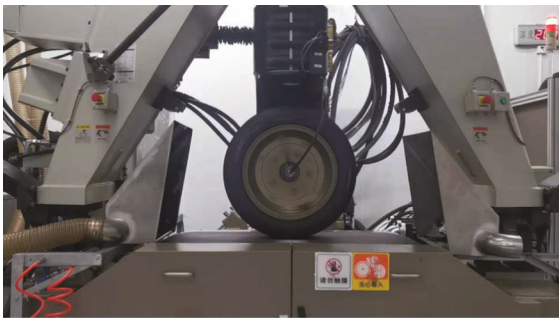In the section, we tested the tire of 215/60R17 specification through MTS Flat-Trac Tire Test Systems which is
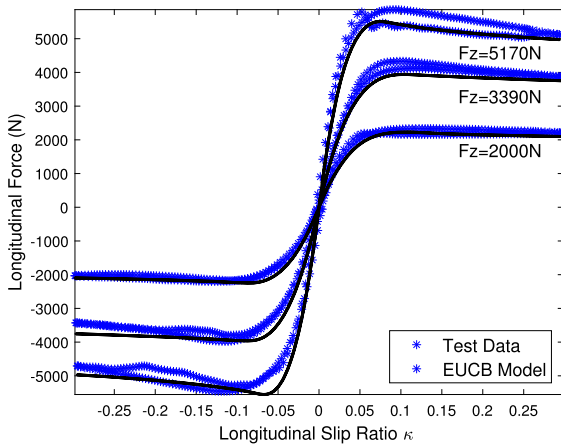
Fig. 14 Tire slip test system

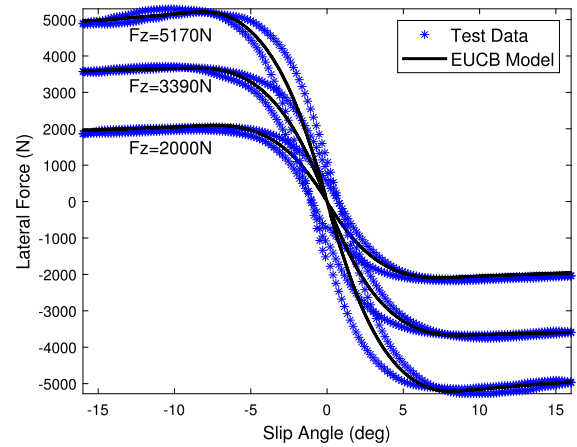**Fig. 15** Longitudinal force at pure slip condition
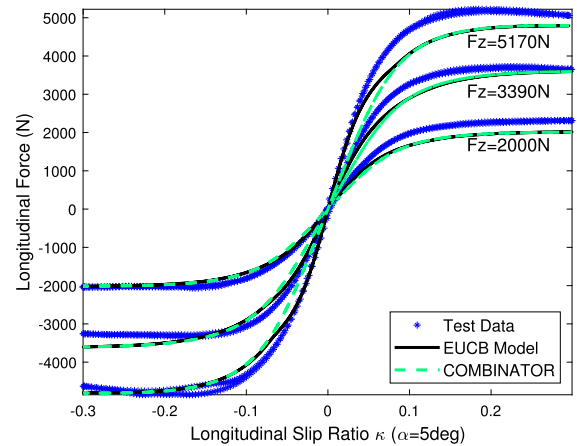

Fig. 16 Lateral force at pure slip condition

Fig. 17 Longitudinal force comparisons between EUCB model and COMBINATOR model at 5° slip angle

industry-recognized tire test system. And tires of this specification are often used in practice and made by Wanli Tire Corporation Limited. The test content is the tire force and moment characteristics on dry roads under steady-state conditions, including test data of pure cornering, pure longitudinal slip and combined-slip conditions under different loads. Figure 14 shows the tire test system used in the section.

5.2 Experiment validation for pure and combined slip conditions

In the section, tire test data of 215/60R17 specification are used to validate the EUCB model proposed above for pure and combined slip conditions. Firstly, the method of nonlinear least squares fitting is used to identify the parameters expressing friction characteristics, cornering stiffness and longitudinal slip stiffness from pure slip condition. Then, the characteristic

parameters are brought into the proposed model with dynamic friction to predict the tire forces.

Figures 15 and 16 show the fitting results between test data and the proposed model above at three different loads under pure slip conditions. The results indicate the model could express pure lateral and longitudinal forces accurately.

Figures 17, 18, 19 and 20 indicate the compared results between EUCB model and COMBINATOR model at two slip angles and three loads. The green dashed lines denote the longitudinal and lateral forces obtained by COMBINATOR model, and the black lines denote the forces obtained by EUCB model proposed.

The results show that both models could describe tire forces well. The comparisons indicate that two
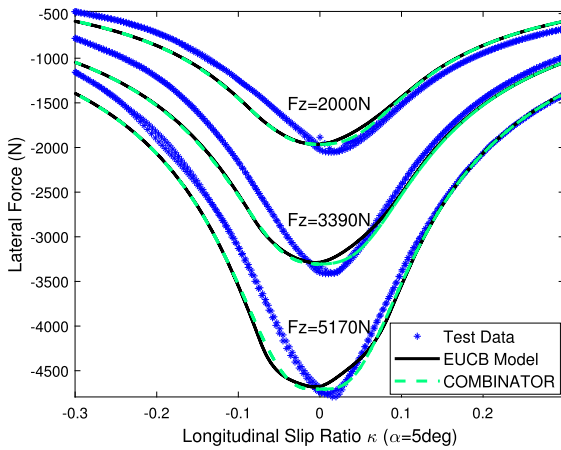
Fig. 18 Lateral force comparisons between EUCB model and COMBINATOR model at 5° slip angle
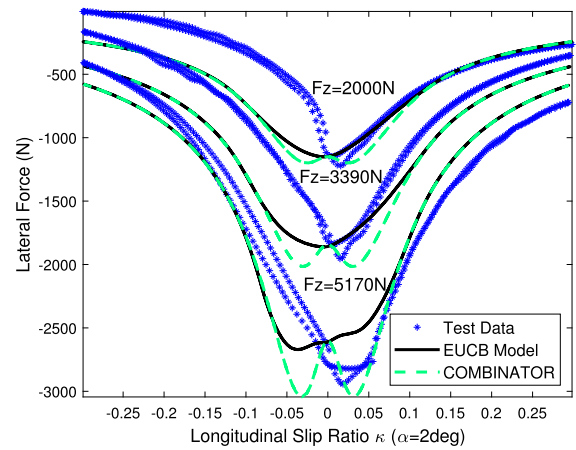

Fig. 20 Lateral force comparisons between EUCB model and COMBINATOR model at 2° slip angle
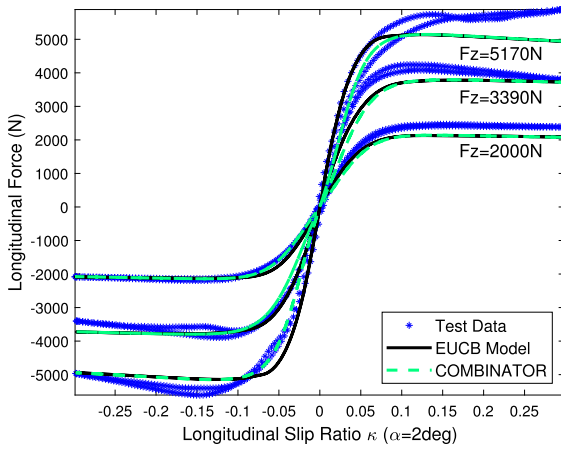

Fig. 19 Longitudinal force comparisons between EUCB model and COMBINATOR model at 2° slip angle
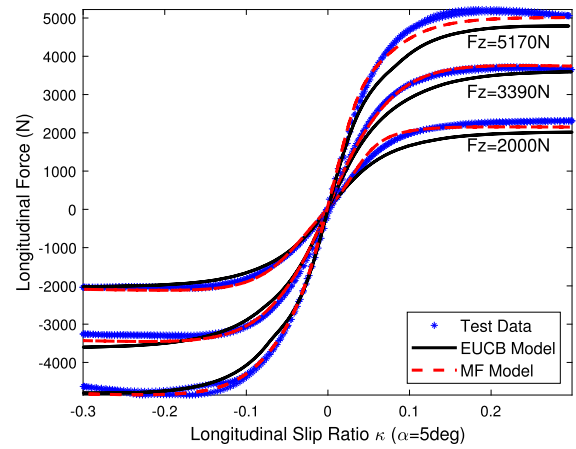

Fig. 21 Longitudinal force comparisons between EUCB model and MF model at 5° slip angle

models are similar at large slip condition and different obviously at small slip condition. The slip direction is viewed as the direction of resultant shear force in COMBINATOR model [24,25]. Therefore, the similarity is because the slip direction is the same as the direction of resultant shear force at large slip condition [15]. The difference is mainly because the direction of resultant shear force of the two models are different at small slip condition. The mathematical expressions of COMBINATOR model is shown in Appendix A.

Figures 21, 22, 23 and 24 indicate the compared results between EUCB model and MF model. The red dashed lines denote forces obtained by MF model, and the black denote the forces obtained by EUCB model. The results show that MF model has better fitting effect

than EUCB model on the whole. The reason is that MF empirical tire model is obtained from tire test data under pure slip and combined conditions, and EUCB model is obtained from tire test data under pure slip. The MF model has high accuracy and is suitable for tire dynamics simulation. Compared with the MF model, the EUCB model has fewer parameters, more concise expression, and lower computation load. Therefore, the EUCB model is suitable for controller design, model-based online estimation and theoretical derivation and analytical solution in vehicle dynamics research.

Combined with the relevant theoretical knowledge of tires, it can be seen that there are two main reasons that limit the accuracy of the EUCB model. One reason is inaccurate pressure distribution of contact patch.
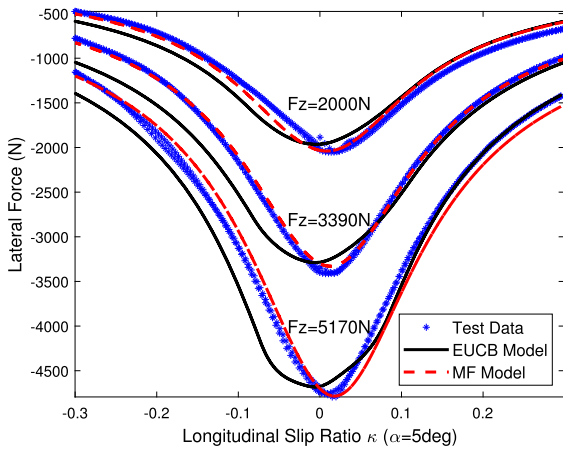
Fig. 22 Lateral force comparisons between EUCB model and MF model at 5° slip angle
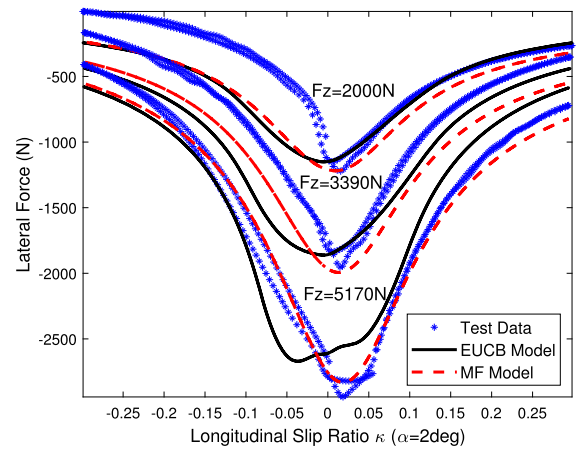

Fig. 23 Longitudinal force comparisons between EUCB model and MF model at 2° slip angle

Fig. 24 Lateral force comparisons between EUCB model and MF model at 2° slip angle
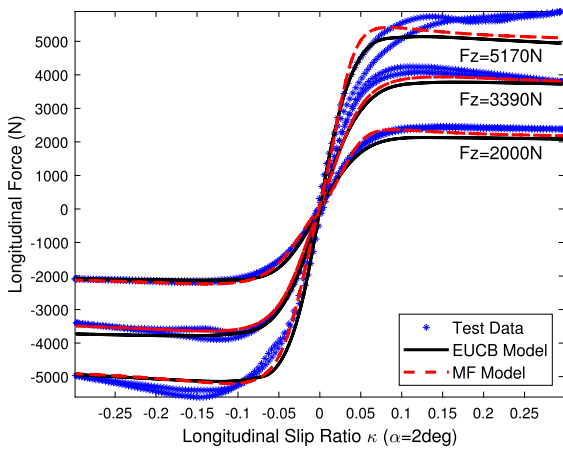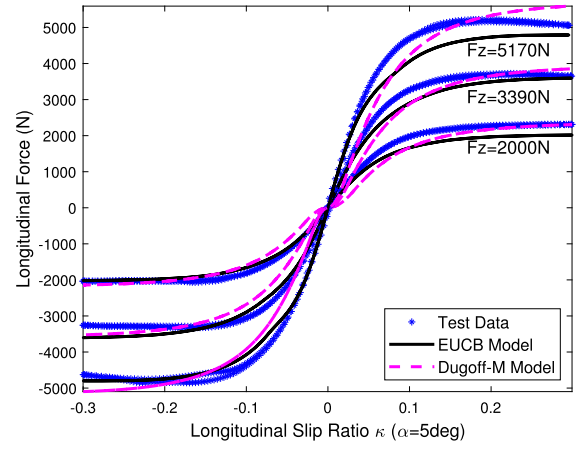

Fig. 25 Longitudinal force comparisons between EUCB model and Modified Dugoff model at 5° slip angle

Fig. 26 Lateral force comparisons between EUCB model and Modified Dugoff model at 5° slip angle

There is a big difference between this pressure distribution and the test results. The other reason is the effect of carcass elasticity on the mechanical properties of tires. When the carcass is elastic, the cornering stiffness of the tire under the combined slip conditions is affected by the longitudinal slip rate or longitudinal force, which is different from the assumption of a rigid carcass [7].

Figures 25, 26, 27 and 28 indicate the compared results between EUCB model and Modified Dugoff model. The pink dashed lines denote forces obtained by Modified Dugoff model, and the black denote the forces obtained by EUCB model. The results show that EUCB model has better fitting effect than Modified Dugoff model on the whole. And the lateral forces calculated by Modified Dugoff model have a large devi-
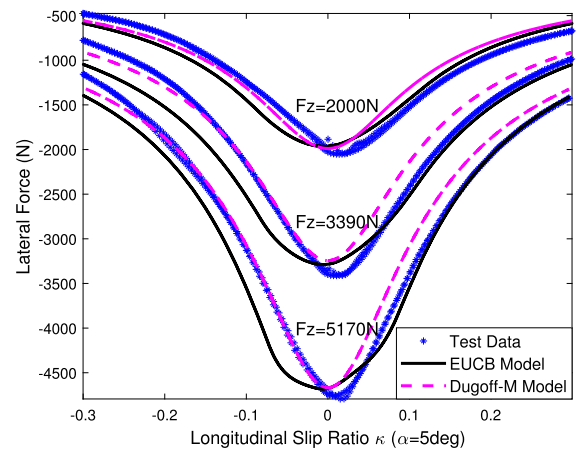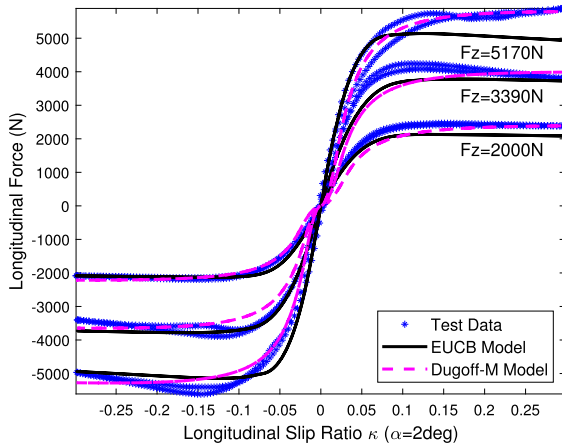
Fig. 27 Longitudinal force comparisons between EUCB model and Modified Dugoff model at 2° slip angle
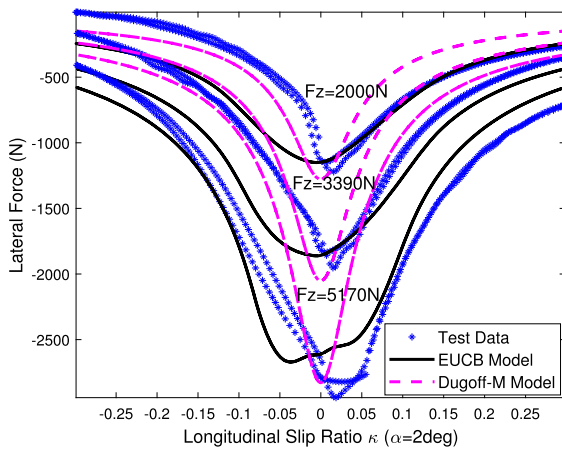

Fig. 28 Lateral force comparisons between EUCB model and Modified Dugoff model at 2° slip angle

ation from the test data at 2° slip angle. This may be caused by anisotropy of tire stiffness. Combined with the previous theoretical analysis, it can be seen that the direction of resultant shear force is inconsistent with the direction of the slip velocity under the small slip condition. However, there is a proportional relationship of slip velocity in the Modified Dugoff model. The mathematical expressions of Modified Dugoff model is shown in Appendix A.

As we all known, the Modified Dugoff model is widely used in controller design and model-based online estimation. And accurate tire model is particularly important under extreme conditions of large slip. Thus, the newly proposed model can improve the per-

formance of the vehicle's active safety system under extreme conditions.

To further indicate the fitting accuracy of the above models, the deviations between the predicted and tested results are shown in Table 1, and γ is the camber angle [29].

$$\varepsilon = \sqrt{\frac{\sum_{i=1}^{n} (y_{i,predicted} - y_{i,tested})^2}{\sum_{i=1}^{n} y_{i,tested}^2}} \times 100\% \qquad (44)$$

where ε is the deviations, n is the number of test data points, $y_{i,predicted}$ is the predicted results, and $y_{i,tested}$ is the tested results. From the deviation comparisons, it can be seen that EUCB physical model has higher prediction accuracy than COMBINATOR model and Modified Dugoff model in longitudinal force and lateral force, and has lower fitting accuracy than MF empirical model, which indicates the EUCB model has acceptable fitting accuracy and good predictive effect.

6 Conclusions

An accurate and predictive tire model is very important for vehicle dynamics studies [13]. In the paper, a predictive tire model (the EUCB model) is proposed which can describe tire forces accurately under combined conditions based on pure slip test. Some conclusions are summarized as follows:

Firstly, the resultant shear force shouldn't be the algebraic sum of the shear stress integrals in sliding and adhesion regions but the vector sum when tire slip stiffness is anisotropic. The vector distribution relationship considering anisotropic tire stiffness accurately describes the variation of shear forces from the physical mechanism.

Secondly, the proposed model is verified by test data at different angles and loads and compared with COMBINATOR model, MF model and Modified Dugoff model. The result shows the model has good accuracy even if a parabolic distribution on vertical load over the contact patch is adopted in the modelling.

Thirdly, the proposed model still needs to further improve accuracy and incorporate some uncertainty caused by unmodeled factors (such as the elasticity of carcass, etc.), and more test data need to be collected to further validate the model.

Table 1 Deviation comparisons among MF model, COMBINATOR model, modified Dugoff model and EUCB model under combined condition

Combined slip conditions			Deviation(%)							
			F_x				F_y			
$\alpha(°)$	$\gamma(°)$	κ	MF	Combinator	Modified dugoff	EUCB	MF	Combinator	Modified dugoff	EUCB
2	0	$-0.3\sim0.3$	7.44	9.23	7.32	8.65	17.20	22.93	34.52	20.78
5	0	$-0.3\sim0.3$	3.72	9.55	10.53	8.03	4.40	8.80	7.28	9.01
Average Deviation			5.58	9.39	8.93	8.34	10.80	15.87	20.90	14.90

Further, in practical application, the proposed model is more suitable for the analytical solution of vehicle system, controller design and model-based online estimation than other commonly used tire models due to its simple expression and acceptable accuracy.

Data Availability Statement The data supporting the conclusions of this article are available from the corresponding author on reasonable request.

Declarations

Conflict of interest The authors declare that they have no conflict of interest.

Appendix A: mathematical expressions of COMBINATOR model and Modified Dugoff model

1. COMBINATOR model

   Lateral force and longitudinal force [21] under combined slip condition are:

   $$\begin{cases} F_y = F \sin \alpha \\ F_x = F \cos \alpha \end{cases} \tag{45}$$

   where F is the magnitude of the resultant shear force, β_s is the direction angle of resultant shear force, and their expressions are [21]:

   $$F = 0.5(F_{x0} + F_{y0}) + 0.5(F_{x0} - F_{y0})cos(2\beta_s) \tag{46}$$

   $$\beta_s = \arctan(\frac{V_{sy}}{V_{sx}}) \tag{47}$$

   where F_{x0} is longitudinal tire force for pure-slip, F_{y0} is lateral tire force for pure-slip, V_{sx} is the longitudinal slip velocity of tire, and V_{sy} is the lateral slip velocity [21]. F_{x0} and F_{y0} can be obtained separately through MF model under pure slip condition.

2. Modified Dugoff model

2.1 Modified Dugoff model at pure-slip conditions

The lateral tire force and longitudinal tire force [18] are given by [18]:

$$
\begin{cases}
F_{0y} = k_y \dfrac{\tan(\alpha)}{1 + \sigma_x} f(\lambda) \\
F_{0x} = k_x \dfrac{\sigma_x}{1 + \sigma_x} f(\lambda)
\end{cases}
\tag{48}
$$

where $f(\lambda)$ and λ are given by:

$$
F(\lambda) = \begin{cases} (2 - \lambda)\lambda, & \lambda \le 1 \\ 1, & \lambda > 1 \end{cases}
\tag{49}
$$

$$
\lambda = \frac{\mu_{x/y} F_z (1 + \sigma_x)}{2\sqrt{(k_x \sigma_x)^2 + (k_y \tan(\alpha))^2}}
\tag{50}
$$

σ_x is the longitudinal slip ratio [18] of tire and its expression is:

$$
\sigma_x = \begin{cases} -\dfrac{V_{sx}}{\Omega R_e}, & during\ acceleration \\ -\dfrac{V_{sx}}{V_x}, & during\ braking \end{cases}
\tag{51}
$$

The friction coefficients [18] are expressed as:

$$
\begin{cases}
\mu_y = \mu_{yp} - (\mu_{yp} - \mu_{ymin}) S_s \\
\mu_x = \mu_{xp} - (\mu_{xp} - \mu_{xmin}) S_\alpha
\end{cases}
\tag{52}
$$

where μ_{yp} is corrected maximum lateral friction coefficient, μ_{xp} is corrected maximum longitudinal friction coefficient, μ_{ymin} is minimum lateral friction coefficient, μ_{xmin} is minimum longitudinal friction coefficient, S_s is absolute longitudinal slip ratio, S_α is absolute lateral slip ratio [18]. μ_{yp} and μ_{xp} are expressed as [18]:

$$
\begin{cases}
\mu_{yp} = IF_y \mu_{ymax} \\
\mu_{xp} = IF_x \mu_{xmax}
\end{cases}
\tag{53}
$$

IF_y and IF_x are increase factors. S_s and S_a are expressed as [18]:

$$
\begin{cases}
S_s = |s| \\
S_\alpha = \min\left(1, \left|\dfrac{V \sin(\alpha)}{V \cos(\alpha), \Omega R_e}\right|\right)
\end{cases}
\tag{54}
$$

IF_x, IF_y, μ_{xmin}, μ_{ymin}, μ_{xmax}, μ_{ymax} can be obtained from MF tire parameters as Ref [18].

2.2 Modified Dugoff model at combined-slip conditions

Lateral force and longitudinal force [18] under combined slip condition are:

$$
\begin{cases}
F_y = F_{0y} \sin\beta \\
F_x = F_{0x} \cos\beta
\end{cases}
\tag{55}
$$

where the angle β [18] is expressed as:

$$
\beta = \arctan\left(\frac{V_{sy}}{V_{sx}}\right)
\tag{56}
$$

References

1. Cao, D., Tang, B., Jiang, H., et al.: Study on low-speed steering resistance torque of vehicles considering friction between tire and pavement. Appl. Sci. **9**, 1015 (2019)
2. Steindl, A., Edelmann, J., Plöchl, M.: Limit cycles at oversteer vehicle. Nonlinear Dyn. **99**, 313–321 (2020)
3. Sun, X., Hu, W., Cai, Y., et al.: Identification of a piecewise affine model for the tire cornering characteristics based on experimental data. Nonlinear Dyn. **101**, 857–874 (2020)
4. Guo, K.: Handling Dynamics Theory of Automobiles, 1st edn. Jiangsu Press of Science and Technology, Nanjing (2011)
5. Pacejka, H.B.: In-plane and out-of-plane dynamics of pneumatic tyres. Veh. Syst. Dyn. **10**(4–5), 221–251 (1981)
6. Pacejka, H.B.: Tire and Vehicle Dynamics, 3rd edn. ButterworthHeinemann, Oxford (2012)
7. Xu, N.: Study on the Steady State Tire Model under Combined Conditions. Ph.D. thesis, Jilin University, Changchun (2012)
8. Barbosa, B.H.G., Xu, N., Askari, H., et al.: Lateral force prediction using Gaussian process regression for intelligent tire systems. IEEE Trans. Syst. Man Cybern. Syst. 1–12 (2021)
9. Tönük, E., Ünlüsoy, Y.S.: Prediction of automobile tire cornering force characteristics by finite element modeling and analysis. Comput. Struct. **79**(13), 1219–1232 (2001)
10. Davoodabadi, I., Ramezani, A.A., Mahmoodi-k, M., et al.: Identification of tire forces using Dual Unscented Kalman Filter algorithm. Nonlinear Dyn. **78**, 1907–1919 (2014)
11. López, A., Olazagoitia, J., Moriano, C.: Nonlinear optimization of a new polynomial tyre model. Nonlinear Dyn. **78**, 2941–2958 (2014)
12. Guo, K., Ren, L.: A unified semi-empirical tire model with higher accuracy and less parameters. SAE Trans. **108**, 1513–1520 (1999)
13. Xu, N., Guo, K., Zhang, X.: UniTire model for tire forces and moments under combined slip conditions with anisotropic tire slip stiffness. SAE Int. J. Commer. Veh. **6**(2), 315–324 (2013)
14. Xu, N., Guo, K.: Modeling combined braking and cornering forces based on pure slip measurements. SAE Int. J. Commer. Veh. **5**, 470–482 (2012)
15. Guo, K., Xu, N., Lu, D., et al.: A model for combined tire cornering and braking forces with anisotropic tread and carcass stiffness. SAE Int. J. Commer. Veh. **4**, 84–95 (2011)
16. Guo, K., Lu, D.: UniTire: unified tire model for vehicle dynamic simulation. Veh. Syst. Dyn. **45**(sup1), 79–99 (2007)
17. Goh, J.Y., Gerdes, J.C.: Simultaneous stabilization and tracking of basic automobile drifting trajectories. In: 2016 IEEE Intelligent Vehicles Symposium (IV). 597–602 (2016)
18. Gim, G., Nikravesh, P.E.: An analytical model of pneumatic tyres for vehicle dynamics simulations. Part 2: comprehensive slips. Int. J. Veh. Des. **12**(1), 19–39 (1991)

19. Gim, G.: Vehicle dynamic simulation with a comprehensive model for pneumatic tires. Ph.D. thesis, The University of Arizona, Tucson (1988)

20. Dugoff, H., Fancher, P., Segel, L.: Tire Performance Characteristics Affecting Vehicle Response to Steering and Braking Control Inputs. Highway Safety Research Institute of Science and Technology. The University of Michigan, Michigan (1969)

21. Ding, N., Taheri, S.: A modified dugoff tire model for combined-slip forces. Tire Sci. Technol. **38**(3), 228–244 (2010)

22. Chen, L., Bian, M., Luo, Y., et al.: Maximum tire road friction estimation based on modified dugoff tire model. In: 2013 International Conference on Mechanical and Automation Engineering. 56–61 (2013)

23. Bian, M., Chen, L., Luo, Y., et al.: A dynamic model for tire/road friction estimation under combined longitudinal/lateral slip situation. SAE Technical Paper. 1 (2014)

24. Schuring, D.J., Pelz, W., Pottinger, M.G.: A model for combined tire cornering and braking forces. SAE Trans. **105**, 113–25 (1996)

25. Pottinger, M., Pelz, W., Falciola, G.: "Effectiveness of the Slip Circle, "COMBINATOR", Model for Combined Tire Cornering and Braking Forces When Applied to a Range of Tires". SAE Technical Paper, 982747 (1998)

26. Zhuang, Y., Guo, K.: Influence of dynamic friction property on the combined side and longitudinal slip properties of tire. J. Jilin Univ. (Eng. Technol. Ed). **38**, 11–14 (2008)

27. Guo, K., Zhuang, Y., Lu, D., et al.: A study on speed-dependent tyre-road friction and its effect on the force and the moment. Veh. Syst. Dyn. **43**, 329–340 (2005)

28. Guo, K., Yuan, Z., Lu, D., et al.: Speed prediction ability of unitire steady-state model. J. Jilin Univ. (Eng. Technol. Ed). **35**, 457–461 (2005)

29. Xu, N., Lu, D., Ran, S., et al.: A predicted tire model for combined tire cornering and braking shear forces based on the slip direction. 2011 Int. Conf. Electron. Mech. Eng. Inf. Technol. 2073–2080 (2011)